Supporting Information for

Characterization of Saddled Nickel(III) Porphyrin Cation Radical :The NMR Explicative Model for Ferromagnetically Coupled Metalloporphyrin Radical**

Ru-Jen Cheng*, Chiao-Han Ting, Ten-Chih Chao, Tzu-Hsien Tseng and Peter P.-Y. Chen*

Department of Chemistry, National Chung-Hsing University,Taichung, Taiwan 402

Correspondence to: pychen@dragon.nchu.edu.tw

Table of Contents

1. Experimental Section **S4**

2. Equations for paramagnetic NMR shifts **S5**

3. Computational Methods **S6**

DFT calculation

DFT calculated contact shifts

4. Orbital symmetry for metalloporphyrins **S7**

Table S1. Correlation table for the molecular orbitals of metalloporphyrins

5. Absorption spectra **S8**

Figure S1. Absorption spectral change for two electron oxidation of Ni^{II}(OETPP)

6. Crystallographic Experimental Tables **S9**

Table S2. Crystal data for Ni^{III}(OETPP·)$(Br)_2$

Table S3. Bond lengths [Å] and angles [°] for Ni^{III}(OETPP·)$(Br)_2$

Table S4. Atomic coordinates for Ni^{III}(OETPP·)$(Br)_2$

Table S5. Crystal data for Ni^{III}(OET(*p*-CH_3)PP·)$(Br)_2$

Figure S2 ORTEP representation of the structure of Ni(OET(*p*-CH_3)PP)$(Br)_2$ with 50% probability ellipsoids. Hydrogens are omitted for clarity.

Table S6. Bond lengths [Å] and angles [°] for Ni^{III}(OET(*p*-CH_3)PP·)$(Br)_2$

Table S7. Atomic coordinates for Ni^{III}(OET(*p*-CH_3)PP·)$(Br)_2$

7. Magnetic data **S21**

Figure S3. Magnetic data for Ni^{III}(OETP(*p*-X)P)$(Br)_2$ (X = H and CH_3)

8. EPR study **S21**

Figure S4. EPR spectrum and simulation

9. ^{1}H NMR studies **S23**

Figure S5. The 400 MHz ^{1}H NMR spectra with Br_2 gradually adding to Ni^{II}(OETPP)

Figure S6. The 400 MHz ^{1}H NMR spectra of Ni^{III}(OETP(*p*-X)P)$(Br)_2$(X = NO_2, CF_3, H, and CH_3)

Figure S7. The 400 MHz ^{1}H and 600 MHz ^{13}C NMR spectrum of Ni^{III}(OETPP·)$(Br)_2$

Figure S8. Plot of isotropic shifts as a function of geometric factor (G)

10. DFT calculation results **S25**

Figure S9. Correlation plot of the calculated Fermi contact spin of HS Ni(III) a_{2u} radical versus isotropic shifts

Table S8. The summary chemical shifts for each component and calculated Fermi contact spin densities for LS Ni(III) a_{1u} radical

Table S9. The summary chemical shifts for each component and calculated Fermi contact spin densities for HS Ni(III) a_{2u} radical

11. Diamagnetic NMR reference complex **S28**

Table S10. ^{1}H and ^{13}C NMR chemical shifts for $[Co(OETPP)(Im)_2](ClO_4)$

12. References **S28**

1. Experimental Section

Materials and Physical Measurements: All reagents are purchased from commercial suppliers, OETPP (dianion of 2,3,7,8,12,13,17,18-octaethyl-5,10,15,20-tetraphenyl-porphyrin) and Ni^{II}(OETPP) are synthesized by reported methods.[1-4] The six-coordinate $Ni^{III}(OETPP^{\cdot})(Br)_2$ can be simply obtained by addition of one equivalent of Br_2 into the benzene solution of Ni^{II}(OETPP) at room temperature.

Magnetic susceptility of powdered samples are recorded by a SQUID system in the temperature range 4-300 K with a external magnetic field of 3000 G. A Suitable crystal is immersed in FOMBLIN®Y under a nitrogen atmophere and mounted on an Oxford Xcalibur Sapphire-3 CCD Gemini diffractometer employing graphite-monochromated Mo-Kα radiation (λ = 0.71073 Å), intensity data are collected with ω scans. The data collection and reduction are performed with the CrysAlisPro software[5] and the absorptions are corrected by SCALE3 ABSPACK multi-scan method.[6] The space group determination is based on a check of the Laue symmetry and systematic absences, and is confirmed using the structure solution. The structure is solved and refined with SHELXTL package.[7] All non-H atoms are located from successive Fourier maps and hydrogen atoms are refined using a riding model. Anisotropic thermal parameters are used for all non-H atoms, and fixed isotropic parameters are used for H atoms.

NMR spectra are obtained by Varian MR 400, Mercury 400 ,and INOVA 600 MHz NMR spectrometer. EPR data are carried out at 77 K by Bruker Model EMX-10/12 spectrometer (Bruker Optic GmbH, Karlsruhe, Germany). EPR simulation is performed by EasySpin[8] shown in Figure S3.

2. Equations for paramagnetic NMR shifts[9-12]

The general expressions of two pseudocontact shifts for the axially symmetric cases, including metal- and ligand-centered terms, are proportional to the anisotropy of magnetic susceptibility, $(\chi_{//} - \chi_{\perp})$.[12]

$$\delta_{dip}^{MC} = \frac{\mu_0}{4\pi}[\frac{1}{3N}(\chi_{//} - \chi_{\perp})\frac{3\cos^2\theta - 1}{r^3}];$$

$$\delta_{dip}^{LC} = \frac{2\Pi}{g_N \beta_N g_e \mu_B}\frac{(\chi_{//} - \chi_{\perp})}{3N}\rho^{\pi};$$

where *N* is Avogadro's number.

For S = 1, assuming $\chi_{XX} = \chi_{YY} = \chi_{\perp}, \chi_{ZZ} = \chi_{//}, g_{XX} = g_{YY}, X = \frac{D}{kT}$ [9]

$$\chi_{ZZ} = \frac{2Ng_{//}^2\beta^2}{kT}(\frac{e^{-X}}{1+2e^{-X}}) \qquad (1)$$

$$\chi_{XX} = \frac{2Ng_{\perp}^2\beta^2}{kTX}(\frac{1-e^{-X}}{1+2e^{-X}}) \qquad (2)$$

Due to D << kT (~ 200 cm^{-1}), the exponential functions of Eqs. (1) and (2) can be reduced as the following expressions by Taylor series:

$$(\frac{e^{-X}}{1+2e^{-X}}) = \frac{1}{3} - \frac{1}{9}X - \frac{1}{54}X^2 + \frac{1}{162}X^3 + ... \sim \frac{1}{3} - \frac{1}{9}X \qquad (3)$$

$$\frac{1}{X}(\frac{1-e^{-X}}{1+2e^{-X}}) = \frac{X}{3} + \frac{1}{18}X^2 - \frac{1}{54}X^3 + ... \sim \frac{1}{3} + \frac{1}{18}X \qquad (4)$$

$$\chi_{//} - \chi_{\perp} = \frac{2\beta^2}{3kT}(g_{//}^2 - g_{\perp}^2)(1 - \frac{g_{//}^2 + \frac{1}{2}g_{\perp}^2}{3(g_{//}^2 - g_{\perp}^2)}\frac{D}{kT}) \qquad (5)$$

When $g_{//}$ is almost equal to $g_{\perp}$, the anisotropy of magnetic susceptibility can be treated as $(\chi_{//} - \chi_{\perp}) = -\frac{g_e^{\ 2}\mu_B^2 DN}{3(kT)^2}$; Accordingly, the metal- and ligand-centered terms are obtained as the following.

$$\delta_{dip}^{M.C.} = -\frac{\mu_0}{4\pi}\frac{{g_e}^2{\mu_B}^2 DG}{9(kT)^2} = -4.486\times10^{-3}(\frac{ppm}{cm^{-1}}\cdot cm^3)\times D\times G;$$

$$\delta_{dip}^{L.C.} = -\frac{g_e\mu_B D(2\Pi)}{9g_N\beta_N(kT)^2}\rho^{\pi} = -48.54(\frac{ppm}{cm^{-1}})\times D\times\rho^{\pi}$$

3. Computational Methods

DFT calculation:

Spin-unrestricted density functional calculations have been carried out for $Ni^{III}(OETPP^{\cdot})(Br)_2$. Molecular geometries were transferred from the crystal structures $Ni^{III}(OETPP^{\cdot})(Br)_2$. The molecular orbitals and spin states were labeled with D_{2d} symmetry for saddled six-coordinate $Ni^{III}(OETPP^{\cdot})(Br)_2$. All the calculations reported in this paper were performed by the Amsterdam density functional (ADF) program package.[13] The all-electron TZP basis sets for paramagnetic NMR data were used for all atoms in the calculations, in which the uncontracted triple-ζ STO basis set, was augmented with one 2p polarization function, one 3d function for carbon and nitrogen, one 4p function for Nickel, and one 4d function for Bromine.[14] The LSD exchange-correlation potential of Vosko-Wilk-Nusair (VWN) was used in all cases, along with the nonlocal Becke exchange correction and nonlocal Perdew correlation.

DFT calculated contact shifts:

Although the DFT calculated contact shifts can be obtained by direct applying the equation of contact term, for most sites these values are already higher than their corresponding isotropic shifts. It is because that the Fermi density is not calculated exactly at the center of the nucleus (r = 0), but at a small sphere containing the center of a nucleus (r = 0 + dr). These direct DFT calculated contact shifts are apparently overestimated and needed to be calibrated with the experimental data. This strategy has been well applied for the interpretation of isomer shifts in Mössbauer spectroscopy. [15]

4. Orbital symmetry for metalloporphyrins

Table S1. Correlation table for the molecular orbitals of metalloporphyrin[a] [16]

	D_{4h}	D_{2h}	D_{2d}[b]	C_{4v}	C_{2v}
Metal					
$d_{x}2-_{y}2$	b_{1g}	a_g	$b_2(b_1)$	b_1	$a_1(a_2)$
d_z2	a_{1g}	a_g	a_1	a_1	a_1
d_{xz}, d_{yz}	e_g	b_{2g}, b_{3g}	e	e	b_1, b_2
d_{xy}	b_{2g}	b_{1g}	$b_1(b_2)$	b_2	$a_2(a_1)$
Porphyrin					
LUMO	e_g	b_{2g}, b_{3g}	e	e	b_1, b_2
HOMO	a_{1u}	a_u	b_1	a_2	a_2
	a_{2u}	b_{1u}	b_2	a_1	a_1
HOMO-1	e_g	b_{2g}, b_{3g}	e	e	b_1, b_2

[a] Defining *x* and *y* axes as lying in the porphyrin plane along trans pyrrole nitrogens. [b] Symmetry representations for ruffle-shaped deformation are given in the parentheses.

5. Absorption spectra

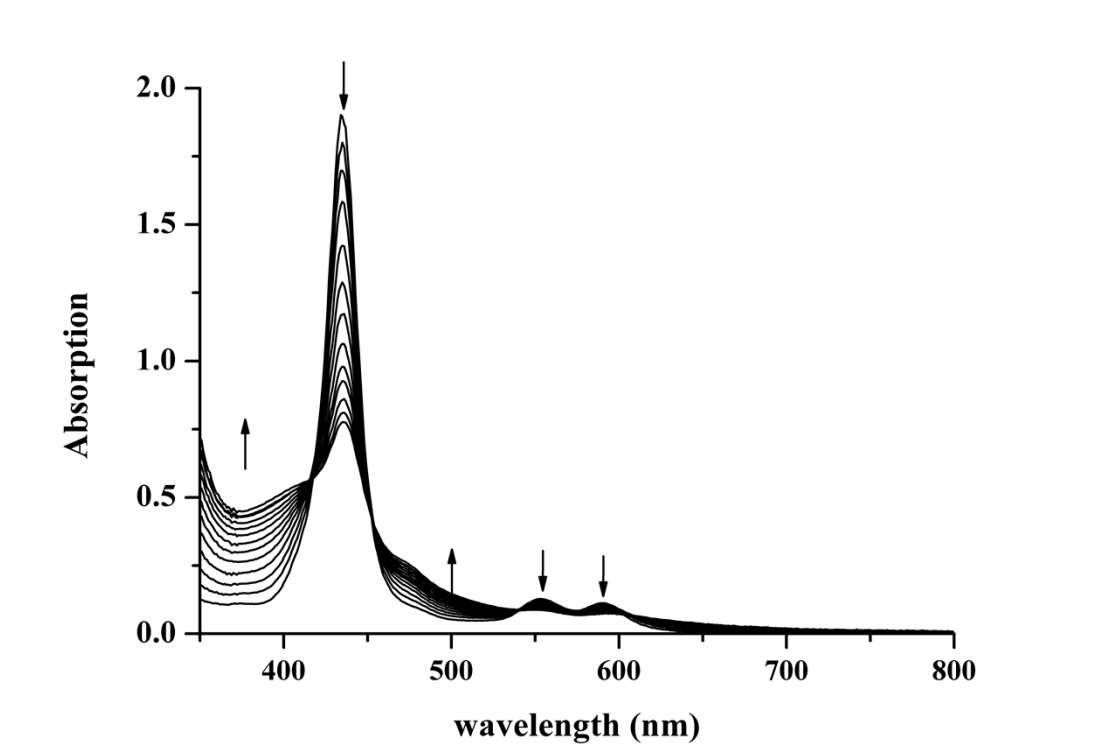

Figure S1. Absorption spectral changes of Ni^{II}(OETPP) upon two-electron oxidation with Br_2 in the solution of benzene at room temperature.

6. Crystallographic Experimental Tables

Table S2. Crystal data of $Ni^{III}(OETPP\cdot)(Br)_2$

Identification code	$Ni(OETPP\cdot)(Br)_2$.	
Chemical formula	$C_{60}\ H_{60}\ Br_2\ N_4\ Ni$	
Formula Mass	1055.65	
Temperature	100(2) K	
Wavelength	0.71073 Å	
Crystal system	Cubic	
Space group	I -4 3 d	
Unit cell dimension	a = 25.945 Å	α = 90°.
	b = 25.945 Å	β = 90°.
	c = 25.945 Å	γ = 90°.
Volume	17464.7 $Å^3$	
Z	12	
Radiation type	MoKα	
Absorption coefficient	1.744 mm^{-1}	
Reflections collected	8564	
Independent reflections	2825 [R(int) = 0.0578]	
Goodness-of-fit on F^2	0.976	
Final R indices [I > 2σ (I)]	R1 = 0.1010, wR2 = 0.2663	
R indices (all data)	R1 = 0.1731, wR2 = 0.2819	
CCDC number	CCDC 1001656	

Table S3. Bond lengths [Å] and angles [°] for Ni(OETPP·)$(Br)_2$

Br-Ni	2.6716(18)
Ni-N#1	1.977(7)
Ni-N#2	1.977(7)
Ni-N#3	1.977(7)
Ni-N	1.977(7)
Ni-Br#2	2.6716(18)
N-C(4)	1.356(11)
N-C(1)	1.414(12)
C(1)-C(5)#2	1.355(14)
C(1)-C(2)	1.502(14)
C(2)-C(3)	1.343(14)
C(2)-C(12)	1.490(14)
C(3)-C(4)	1.482(13)
C(3)-C(14)	1.525(13)
C(4)-C(5)	1.422(14)
C(5)-C(1)#1	1.355(14)
C(5)-C(6)	1.524(16)
C(6)-C(11)	1.316(18)
C(6)-C(7)	1.563(19)
C(7)-C(8)	1.435(18)
C(7)-H(7A)	0.9500
C(8)-C(9)	1.316(19)
C(8)-H(8A)	0.9500
C(9)-C(10)	1.32(2)
C(9)-H(9A)	0.9500
C(10)-C(11)	1.475(18)
C(10)-H(10A)	0.9500
C(11)-H(11A)	0.9500
C(12)-C(13)	1.469(15)
C(12)-H(12A)	0.9900
C(12)-H(12B)	0.9900
C(13)-H(13A)	0.9800
C(13)-H(13B)	0.9800
C(13)-H(13C)	0.9800
C(14)-C(15)	1.525(18)
C(14)-H(14A)	0.9900

C(14)-H(14B)	0.9900
C(15)-H(15A)	0.9800
C(15)-H(15B)	0.9800
C(15)-H(15C)	0.9800
N#1-Ni-N#2	176.8(5)
N#1-Ni-N#3	90.044(13)
N#2-Ni-N#3	90.044(13)
N#1-Ni-N	90.042(13)
N#2-Ni-N	90.046(13)
N#3-Ni-N	176.8(5)
N#1-Ni-Br#2	88.4(2)
N#2-Ni-Br#2	88.4(2)
N#3-Ni-Br#2	91.6(2)
N-Ni-Br#2	91.6(2)
N#1-Ni-Br	91.6(2)
N#2-Ni-Br	91.6(2)
N#3-Ni-Br	88.4(2)
N-Ni-Br	88.4(2)
Br#2-Ni-Br	180.0
C(4)-N-C(1)	106.4(7)
C(4)-N-Ni	122.6(6)
C(1)-N-Ni	122.1(6)
C(5)#2-C(1)-N	120.1(9)
C(5)#2-C(1)-C(2)	130.6(9)
N-C(1)-C(2)	109.2(8)
C(3)-C(2)-C(12)	127.8(10)
C(3)-C(2)-C(1)	105.0(9)
C(12)-C(2)-C(1)	126.5(9)
C(2)-C(3)-C(4)	109.1(8)
C(2)-C(3)-C(14)	126.2(9)
C(4)-C(3)-C(14)	123.6(9)
N-C(4)-C(5)	121.3(8)
N-C(4)-C(3)	109.6(8)
C(5)-C(4)-C(3)	128.9(8)
C(1)#1-C(5)-C(4)	123.1(9)
C(1)#1-C(5)-C(6)	116.9(10)
C(4)-C(5)-C(6)	119.9(9)
C(11)-C(6)-C(5)	125.1(13)

C(11)-C(6)-C(7)	123.2(12)
C(5)-C(6)-C(7)	111.7(12)
C(8)-C(7)-C(6)	115.8(13)
C(8)-C(7)-H(7A)	122.1
C(6)-C(7)-H(7A)	122.1
C(9)-C(8)-C(7)	116.1(14)
C(9)-C(8)-H(8A)	122.0
C(7)-C(8)-H(8A)	121.9
C(8)-C(9)-C(10)	129.0(14)
C(8)-C(9)-H(9A)	115.5
C(10)-C(9)-H(9A)	115.5
C(9)-C(10)-C(11)	121.0(14)
C(9)-C(10)-H(10A)	119.5
C(11)-C(10)-H(10A)	119.5
C(6)-C(11)-C(10)	114.7(13)
C(6)-C(11)-H(11A)	122.6
C(10)-C(11)-H(11A)	122.6
C(13)-C(12)-C(2)	112.0(8)
C(13)-C(12)-H(12A)	109.2
C(2)-C(12)-H(12A)	109.2
C(13)-C(12)-H(12B)	109.2
C(2)-C(12)-H(12B)	109.2
H(12A)-C(12)-H(12B)	107.9
C(12)-C(13)-H(13A)	109.5
C(12)-C(13)-H(13B)	109.5
H(13A)-C(13)-H(13B)	109.5
C(12)-C(13)-H(13C)	109.5
H(13A)-C(13)-H(13C)	109.5
H(13B)-C(13)-H(13C)	109.5
C(3)-C(14)-C(15)	111.0(10)
C(3)-C(14)-H(14A)	109.4
C(15)-C(14)-H(14A)	109.4
C(3)-C(14)-H(14B)	109.4
C(15)-C(14)-H(14B)	109.4
H(14A)-C(14)-H(14B)	108.0
C(14)-C(15)-H(15A)	109.5
C(14)-C(15)-H(15B)	109.5
H(15A)-C(15)-H(15B)	109.5

C(14)-C(15)-H(15C)	109.5
H(15A)-C(15)-H(15C)	109.5
H(15B)-C(15)-H(15C)	109.5

Symmetry transformations used to generate equivalent atoms:

#1 -x+3/4,z-1/4,-y+1/4 #2 -x+3/4,-z+1/4,y+1/4 #3 x,-y,-z+1/2

Table S4. Atomic coordinates (x 10^4) and equivalent isotropic displacement parameters ($Å^2$x 10^3) for Ni(OETPP)Br_2. U(eq) is defined as one third of the trace of the orthogonalized U^{ij} tensor.

	x	y	z	U(eq)
Br	4780(1)	0	2500	63(1)
Ni	3750	0	2500	38(1)
N	3771(3)	-697(3)	2808(3)	16(1)
C(1)	3974(4)	-1126(3)	2541(4)	21(2)
C(2)	4282(4)	-1451(4)	2908(4)	31(3)
C(3)	4194(4)	-1245(3)	3375(3)	17(2)
C(4)	3871(3)	-778(3)	3315(3)	16(1)
C(5)	3648(4)	-461(4)	3703(4)	30(3)
C(6)	3562(6)	-676(5)	4243(5)	57(2)
C(7)	3217(6)	-1170(5)	4235(5)	57(2)
C(8)	3103(6)	-1392(5)	4728(5)	57(2)
C(9)	3320(6)	-1170(5)	5128(5)	57(2)
C(10)	3628(6)	-766(5)	5142(5)	57(2)
C(11)	3767(6)	-487(5)	4667(5)	57(2)
C(12)	4667(4)	-1854(3)	2767(4)	23(2)
C(13)	5124(4)	-1632(5)	2518(5)	45(3)
C(14)	4464(5)	-1392(5)	3875(4)	43(3)
C(15)	4915(5)	-1032(6)	3985(5)	64(4)

Table S5. Crystal data for $Ni^{III}(OET(p\text{-}CH_3)PP^{\cdot})(Br)_2$.

Identification code	$Ni(OET(p\text{-}CH_3)PP)(Br)_2$	
Empirical formula	C64 H68 Br2 N4 Ni	
Formula weight	1111.75	
Temperature	150(2) K	
Wavelength	0.71073 Å	
Crystal system	Cubic	
Space group	I -4 3 d	
Unit cell dimensions	a = 26.4497(10) Å	α= 90°.
	b = 26.4497(10) Å	β= 90°.
	c = 26.4497(10) Å	γ = 90°.
Volume	18503.9(12) $Å^3$	
Z	12	
Density (calculated)	1.197 Mg/m^3	
Absorption coefficient	1.649 mm^{-1}	
F(000)	6936	
Crystal size	0.2 x 0.2 x 0.2 mm^3	
Theta range for data collection	2.18 to 25.99°.	
Index ranges	-32<=h<=32, -19<=k<=32, -32<=l<=28	
Reflections collected	49512	
Independent reflections	1613 [R(int) = 0.1021]	
Completeness to theta = 25.99°	99.1 %	
Absorption correction	None	
Refinement method	Full-matrix least-squares on F^2	
Data / restraints / parameters	1613 / 0 / 161	
Goodness-of-fit on F^2	0.898	
Final R indices [I>2sigma(I)]	R1 = 0.0461, wR2 = 0.1272	
R indices (all data)	R1 = 0.0591, wR2 = 0.1342	
Absolute structure parameter	0.00	
Largest diff. peak and hole	0.451 and -0.406 e.$Å^{-3}$	
CCDC number	CCDC 1021469	

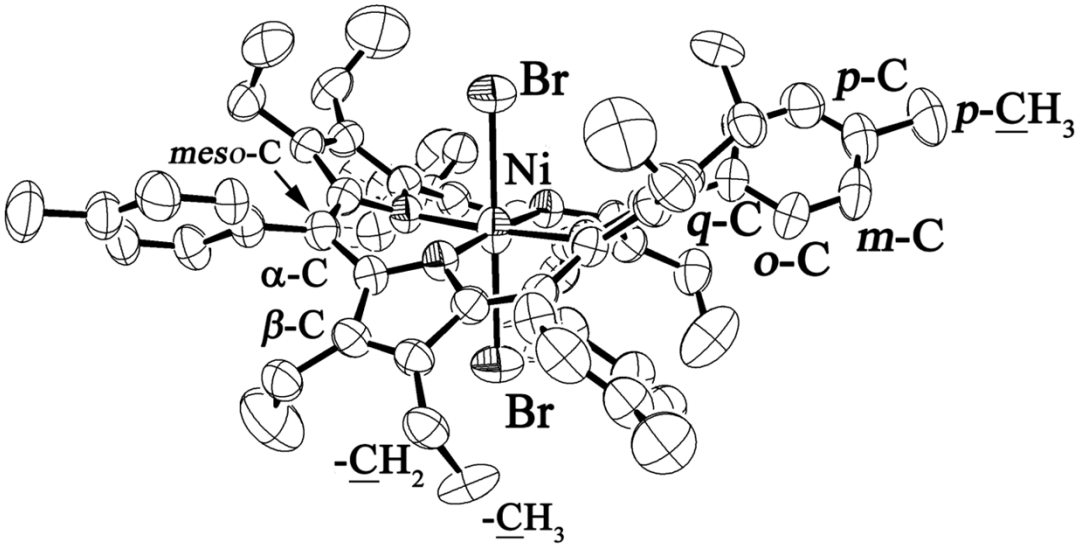

Figure S2. ORTEP representation of the structure of $Ni^{III}(OET(p\text{-}CH_3)PP^{\bullet})(Br)_2$ with 50% probability ellipsoids. Hydrogens are omitted for clarity.

Table S6. Bond lengths [Å] and angles [°] for $Ni^{III}(OET(p\text{-}CH_3)PP\cdot)(Br)_2$

Ni-N#1	1.999(4)
Ni-N#2	1.999(4)
Ni-N#3	1.999(4)
Ni-N	1.999(4)
Ni-Br#1	2.6844(8)
Ni-Br	2.6845(8)
N-C(2)	1.325(7)
N-C(1)	1.385(7)
C(1)-C(5)#1	1.371(7)
C(1)-C(3)	1.478(7)
C(2)-C(5)	1.468(8)
C(2)-C(4)	1.472(7)
C(3)-C(4)	1.359(8)
C(3)-C(6)	1.504(8)
C(4)-C(8)	1.502(8)
C(5)-C(1)#2	1.371(7)
C(5)-C(10)	1.477(8)
C(6)-C(7)	1.559(10)
C(6)-H(6A)	0.9700
C(6)-H(6B)	0.9700
C(7)-H(7A)	0.9600
C(7)-H(7B)	0.9600
C(7)-H(7C)	0.9600
C(8)-C(9)	1.448(14)
C(8)-H(8A)	0.9700
C(8)-H(8B)	0.9700
C(9)-H(9A)	0.9600
C(9)-H(9B)	0.9600
C(9)-H(9C)	0.9600
C(10)-C(11)	1.393(8)
C(10)-C(15)	1.400(8)
C(11)-C(12)	1.375(9)
C(11)-H(11A)	0.9300
C(12)-C(13)	1.395(11)
C(12)-H(12A)	0.9300

C(13)-C(14)	1.349(11)
C(13)-C(16)	1.507(9)
C(14)-C(15)	1.397(9)
C(14)-H(14A)	0.9300
C(15)-H(15A)	0.9300
C(16)-H(16A)	0.9600
C(16)-H(16B)	0.9600
C(16)-H(16C)	0.9600

N#1-Ni-N#2	175.8(3)
N#1-Ni-N#3	90.078(10)
N#2-Ni-N#3	90.077(10)
N#1-Ni-N	90.076(10)
N#2-Ni-N	90.079(10)
N#3-Ni-N	175.8(3)
N#1-Ni-Br#1	92.11(13)
N#2-Ni-Br#1	92.11(13)
N#3-Ni-Br#1	87.89(13)
N-Ni-Br#1	87.89(13)
N#1-Ni-Br	87.89(13)
N#2-Ni-Br	87.89(13)
N#3-Ni-Br	92.11(13)
N-Ni-Br	92.11(13)
Br#1-Ni-Br	180.0
C(2)-N-C(1)	107.0(4)
C(2)-N-Ni	122.7(3)
C(1)-N-Ni	121.8(3)
C(5)#1-C(1)-N	121.6(4)
C(5)#1-C(1)-C(3)	129.2(5)
N-C(1)-C(3)	108.9(4)
N-C(2)-C(5)	121.8(4)
N-C(2)-C(4)	111.4(4)
C(5)-C(2)-C(4)	126.7(4)
C(4)-C(3)-C(1)	106.3(5)
C(4)-C(3)-C(6)	125.9(5)
C(1)-C(3)-C(6)	127.1(5)
C(3)-C(4)-C(2)	105.9(4)
C(3)-C(4)-C(8)	125.0(5)

C(2)-C(4)-C(8)	128.5(5)
C(1)#2-C(5)-C(2)	121.2(4)
C(1)#2-C(5)-C(10)	122.2(5)
C(2)-C(5)-C(10)	116.6(4)
C(3)-C(6)-C(7)	110.3(5)
C(3)-C(6)-H(6A)	109.6
C(7)-C(6)-H(6A)	109.6
C(3)-C(6)-H(6B)	109.6
C(7)-C(6)-H(6B)	109.6
H(6A)-C(6)-H(6B)	108.1
C(6)-C(7)-H(7A)	109.5
C(6)-C(7)-H(7B)	109.5
H(7A)-C(7)-H(7B)	109.5
C(6)-C(7)-H(7C)	109.5
H(7A)-C(7)-H(7C)	109.5
H(7B)-C(7)-H(7C)	109.5
C(9)-C(8)-C(4)	113.0(7)
C(9)-C(8)-H(8A)	109.0
C(4)-C(8)-H(8A)	109.0
C(9)-C(8)-H(8B)	109.0
C(4)-C(8)-H(8B)	109.0
H(8A)-C(8)-H(8B)	107.8
C(8)-C(9)-H(9A)	109.5
C(8)-C(9)-H(9B)	109.5
H(9A)-C(9)-H(9B)	109.5
C(8)-C(9)-H(9C)	109.5
H(9A)-C(9)-H(9C)	109.5
H(9B)-C(9)-H(9C)	109.5
C(11)-C(10)-C(15)	118.8(5)
C(11)-C(10)-C(5)	121.0(5)
C(15)-C(10)-C(5)	120.1(5)
C(12)-C(11)-C(10)	119.6(6)
C(12)-C(11)-H(11A)	120.2
C(10)-C(11)-H(11A)	120.2
C(11)-C(12)-C(13)	121.7(6)
C(11)-C(12)-H(12A)	119.1
C(13)-C(12)-H(12A)	119.1
C(14)-C(13)-C(12)	118.5(6)

C(14)-C(13)-C(16)	120.0(7)
C(12)-C(13)-C(16)	121.4(7)
C(13)-C(14)-C(15)	121.6(7)
C(13)-C(14)-H(14A)	119.2
C(15)-C(14)-H(14A)	119.2
C(14)-C(15)-C(10)	119.6(6)
C(14)-C(15)-H(15A)	120.2
C(10)-C(15)-H(15A)	120.2
C(13)-C(16)-H(16A)	109.5
C(13)-C(16)-H(16B)	109.5
H(16A)-C(16)-H(16B)	109.5
C(13)-C(16)-H(16C)	109.5
H(16A)-C(16)-H(16C)	109.5
H(16B)-C(16)-H(16C)	109.5

Symmetry transformations used to generate equivalent atoms:

#1 y+3/4,-x+5/4,-z+7/4 #2 -y+5/4,x-3/4,-z+7/4 #3 -x+2,-y+1/2,z+0

Table S7. Atomic coordinates (x 10^4) and equivalent isotropic displacement parameters ($Å^2$x 10^3) for Ni^{III}(OET(*p*-CH_3)PP·)$(Br)_2$. U(eq) is defined as one third of the trace of the orthogonalized U^{ij} tensor.

	x	y	z	U(eq)
Ni	10000	2500	8750	61(1)
Br	10000	2500	9765(1)	83(1)
N	9698(2)	3192(2)	8722(2)	50(1)
C(1)	9960(2)	3600(2)	8524(2)	51(1)
C(2)	9212(2)	3271(2)	8630(2)	49(1)
C(3)	9604(2)	3922(2)	8237(2)	51(1)
C(4)	9137(2)	3719(2)	8308(2)	56(1)
C(5)	8816(2)	2958(2)	8860(2)	51(1)
C(6)	9736(3)	4338(2)	7873(2)	65(2)
C(7)	9990(4)	4115(3)	7391(2)	100(2)
C(8)	8665(2)	3888(2)	8041(3)	69(2)
C(9)	8518(5)	3552(6)	7634(5)	156(5)
C(10)	8326(2)	3207(2)	8960(2)	57(1)
C(11)	7881(2)	3029(2)	8742(3)	63(1)
C(12)	7430(2)	3265(3)	8849(3)	78(2)
C(13)	7407(2)	3691(3)	9158(3)	74(2)
C(14)	7840(3)	3872(3)	9358(3)	82(2)
C(15)	8306(2)	3642(2)	9262(2)	61(1)
C(16)	6915(3)	3961(4)	9257(4)	107(3)

7. Magnetic data

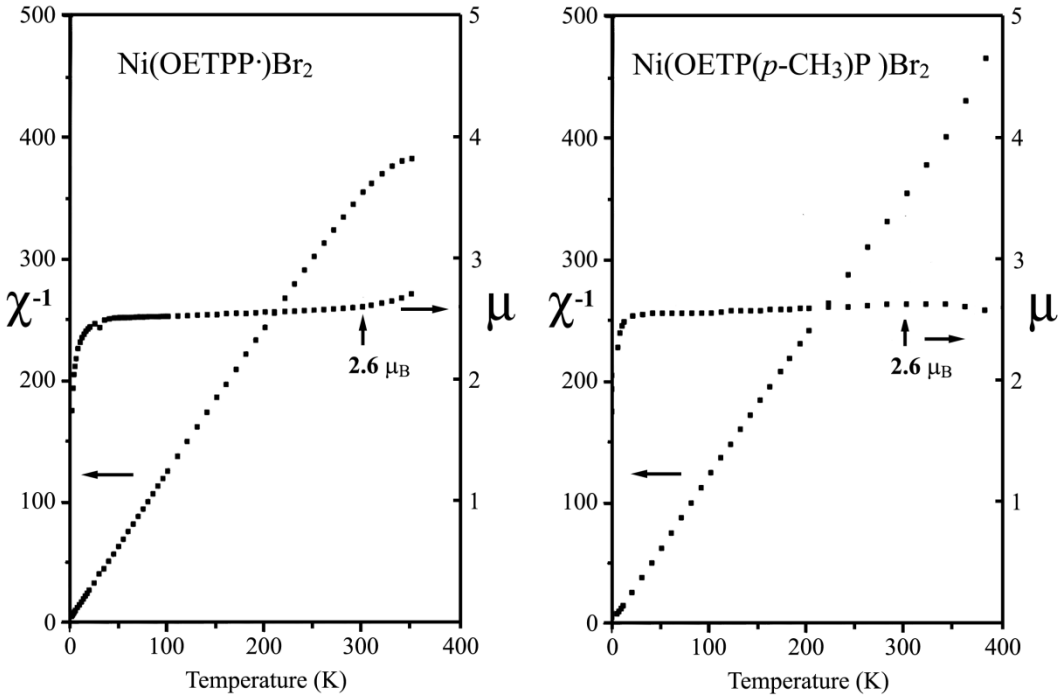

Figure S3. The plot of reciprocal magnetic susceptibility (χ^{-1}) and moment (μ) of $Ni^{III}(OETPP\cdot)(Br)_2$ and $Ni^{III}(OETP(p\text{-}CH_3)P)(Br)_2$ as a function of temperature.

8. EPR simulation

According to the magnetic data, $Ni^{III}(OETPP\cdot)(Br)_2$ is ferromagnetically coupled to a triplet state (S =1), the EPR spectrum can be deduced from the spin Hamiltonian to the following;

$$\hat{H} = \beta g \vec{H} \cdot \vec{S} + D[\hat{S}_z^2 - (1/3)S(S+1)] + E[\hat{S}_x^2 - \hat{S}_y^2]$$

where D and E are the axial and rhombic zero-field splitting parameters, respectively, and g is the average g value. In this simulation, the D value is bet fitted by 0.034 cm^{-1}, and E is zero; g values are best simulated with 2.21, 2.10 and 2.13 denoted to g_x, g_y, g_z, respectively. In this case of small D, the EPR signal has been ascribed to $|-1\rangle \leftrightarrow |0\rangle$, $|0\rangle \leftrightarrow |1\rangle$ transitions along three axes of magnetic field. The corresponding energies of the three microstates of S = 1 were shown in Figure S3.

(a)

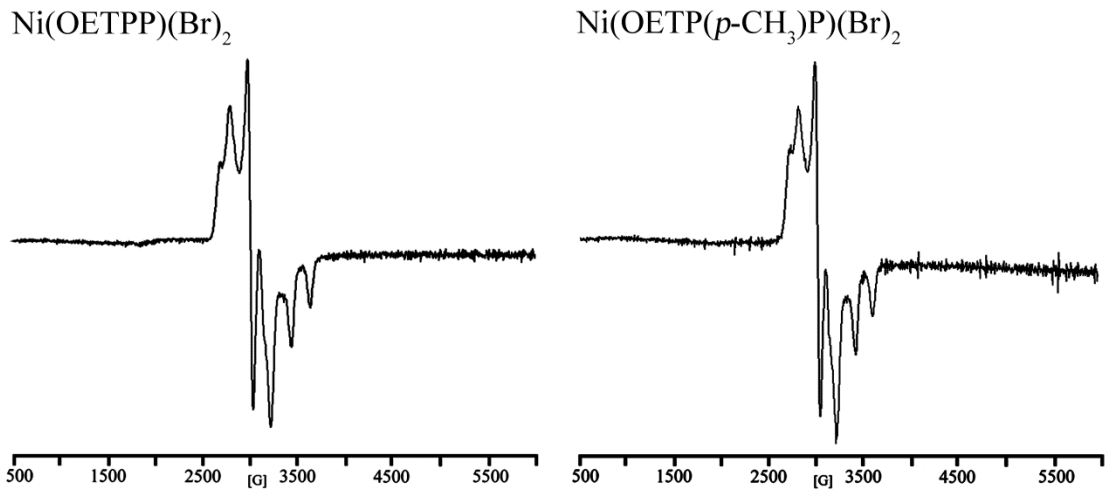

(b)

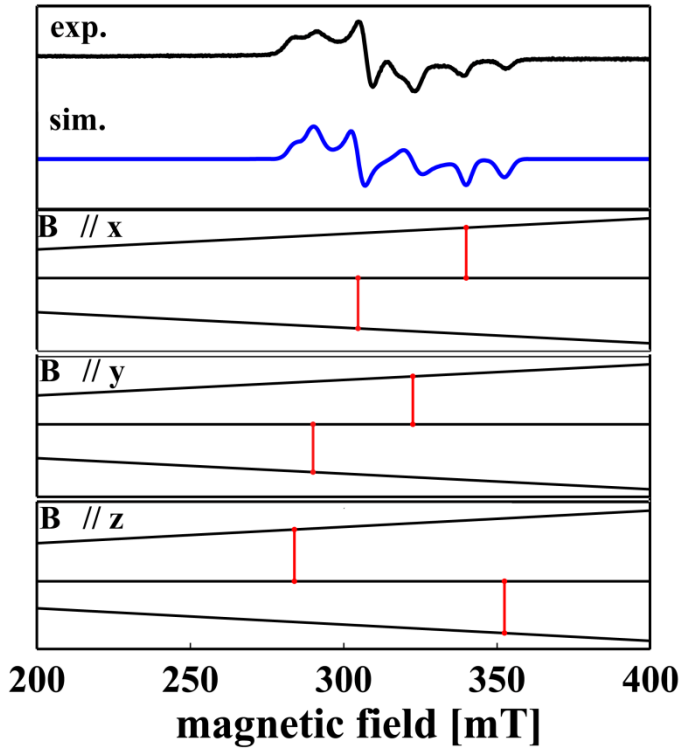

Figure S4. (a) EPR spectra of $Ni^{III}(OET(P\text{-}R)P^{\cdot})(Br)_2$, R= H, and CH_3, at 77K in the solution of benzene (b) EPR spectrum of $Ni^{III}(OETPP^{\cdot})(Br)_2$ at 77K and simulated spectrum with energies of the triplet manifold of S = 1 and magnetic field along the principal molecular axes.

9. ^{1}H NMR studies

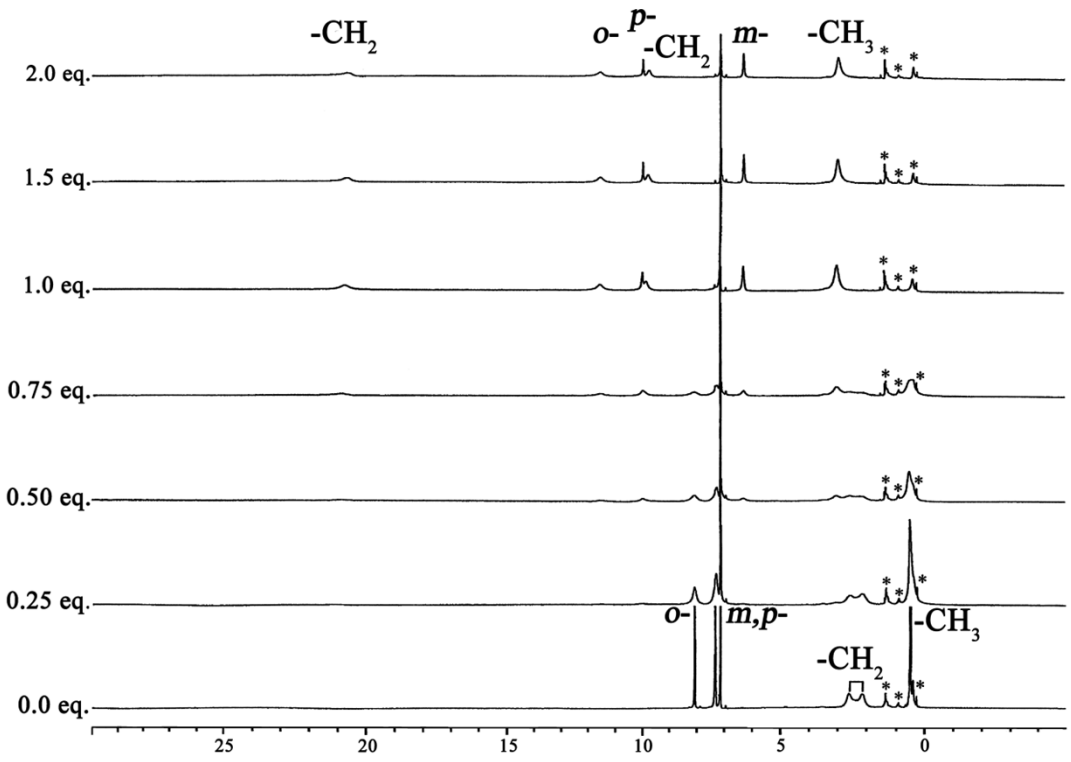

Figure S5. The 400 MHz ^{1}H NMR spectra with Br_2 gradually adding to Ni^{II}(OETPP) in d_6-benzene solution at room temperature. Peaks labeled with star sign correspond to diamagnetic impurities.

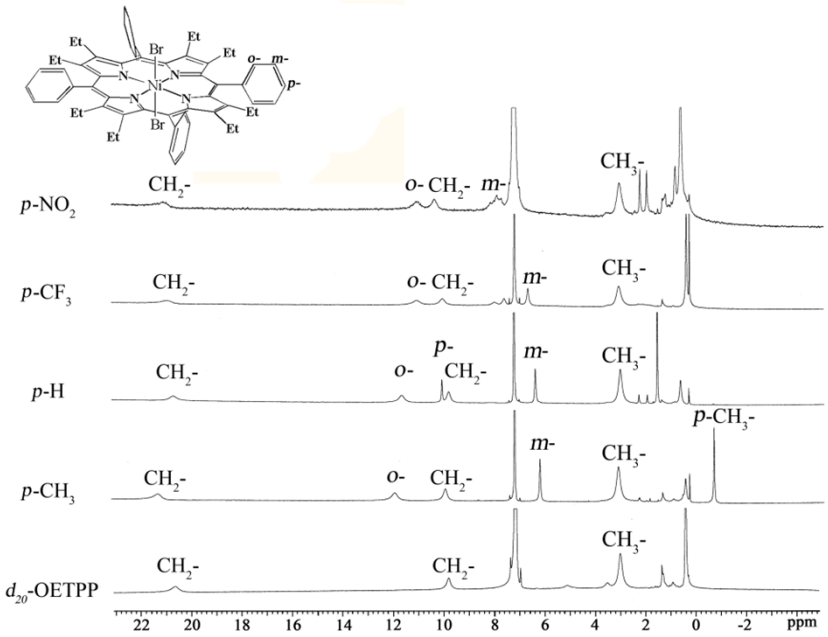

Figure S6 . The 400 MHz ^{1}H NMR spectra of Ni^{III}(OETP(*p*-X)P)$(Br)_2$(X = NO_2, CF_3, H, and CH_3) in d_6-benzene at room temperature.

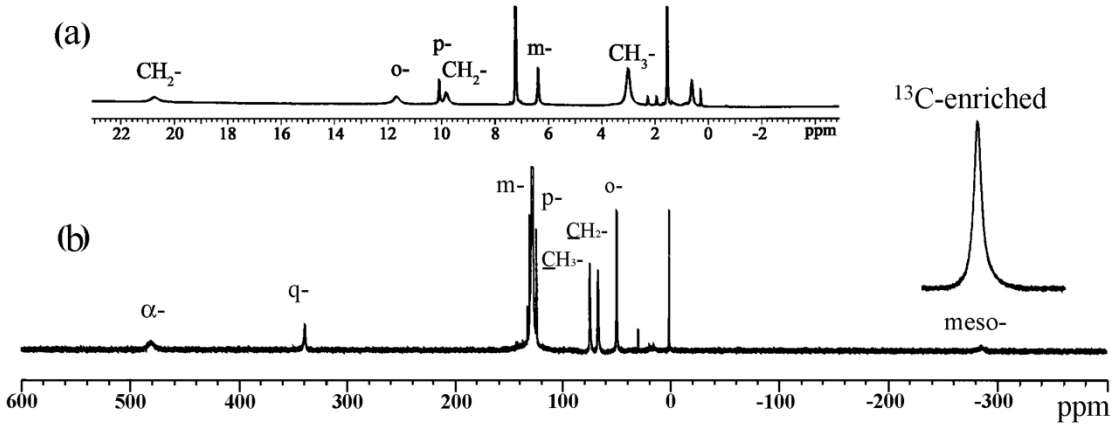

Figure S7. (a) 400 MHz ^{1}H NMR spectrum and (b) 600 MHz ^{13}C NMR spectrum of $Ni^{III}(OETPP^{\cdot})(Br)_2$ in d_6-benzene at room temperature.

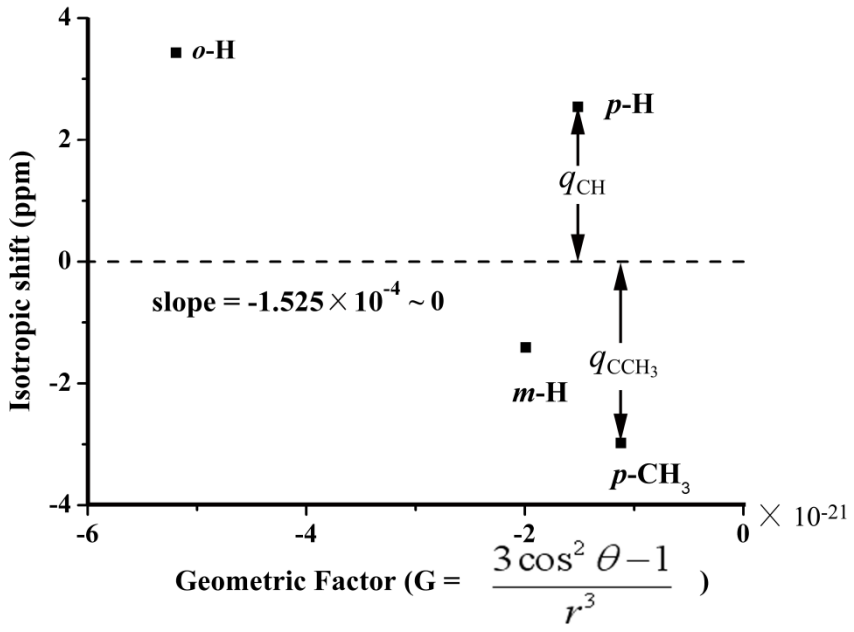

Figure S8. Plot of isotropic shifts at 298K as a function of geometric factor (G) for aryl and *para*-methyl protons in $Ni^{III}(OETP(p\text{-}X)(X = H \text{ or } CH_3)P)(Br)_2$. The dash straight line is evaluated by $\delta_{dip}^{M.C.}$.

10. DFT calculation results

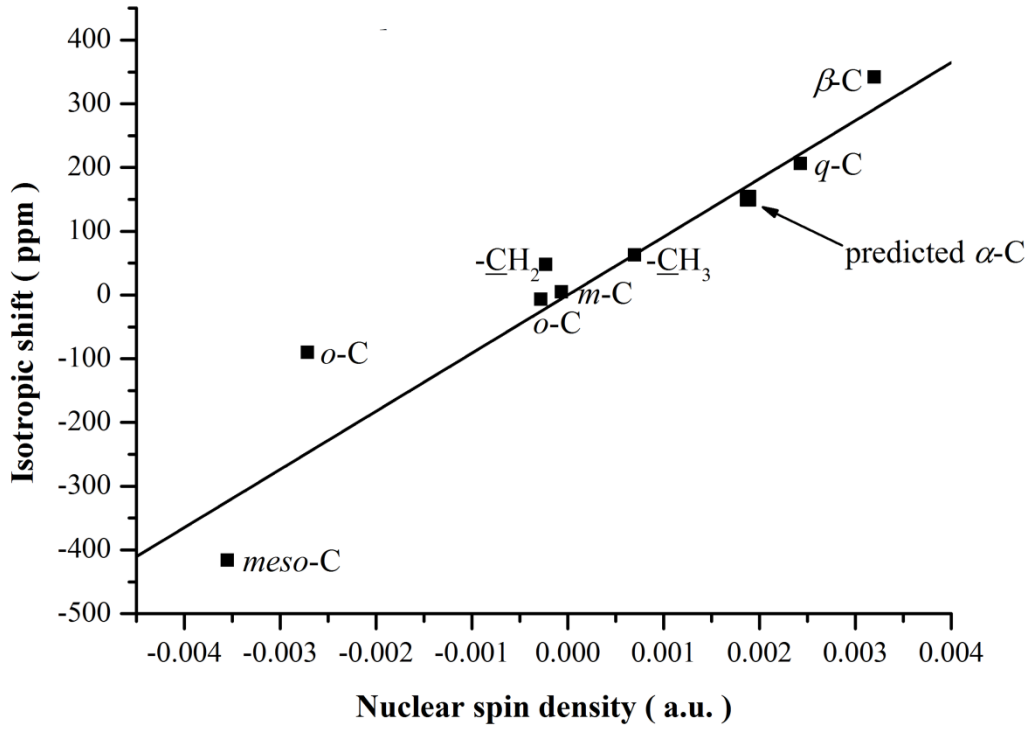

Figure S9. Correlation between the calculated Fermi contact spin densities at each symmetry-distinct atom type and the experimental isotropic shifts of high-spin $Ni^{III}(OETPP\cdot)(Br)_2$ a_{2u} π cation radical complex with fitted slope = 91211 au^{-1}**.** ppm, R^2 = 0.88.

Table S8. Experimental isotropic shifts, estimated pseudocontact shifts and calculated Fermi contact spin densities with corresponding shifts for low-spin $Ni^{III}(OETPP^{\cdot})(Br)_2$ ferromagnetically coupled with a_{1u} π cation radical. (chemical shift in ppm)

	δ_{iso}	$\delta_{dip}^{MC\,a}$	$\delta_{dip}^{LC\,a}$	ρ$^{\pi}$	G (cm^{-3})×10^{21}	$\delta_{con}{}^{b}$	$\rho_{\alpha\beta}{}^{c}$
			Ni(OETPP)Br$_2$, D = 0.034 cm^{-1}				
α-C	342	0.0055	-0.1599	0.0969	-36.02	342.2	0.0126
β-C	nd	0.0016	-0.0116	0.0070	-10.19	nd	-0.0014
meso-C	-416.1	0.0041	0.0375	-0.0227	-26.77	-416.1	-0.0117
q-C	206.2	0.0013	-	-	-8.76	206.2	0.0058
-C$\underline{H}_2$	47.8	0.0005	-	-	-3.43	47.8	-0.0006
-C$\underline{H}_3$	63.1	0.0000	-	-	0.36	63.1	0.0021
o-C	-89.9	0.0008	-	-	-5.08	-89.9	-0.0023
m-C	4.8	0.0004	-	-	-2.73	4.8	0.0000
p-C	-6.8	0.0003	-	-	-2.21	-6.8	-0.0001
-C$\underline{H}_2$	12.98	0.0005	-	-	-3.13	12.98	0.0002
-C$\underline{H}_3$	3.08	-0.0002	-	-	1.17	3.08	0.0001
o-H	3.47	0.0008	-	-	-4.92	3.47	0.0001
m-H	-1.58	0.0003	-	-	-1.89	-1.58	0.0000
p-H	2.34	0.0002	-	-	-1.49	2.34	0.0001

[a] The calculated values of metal-centered and ligand-centered dipolar shifts were based on the zero-field splitting (D) which is mainly estimated from the datum of EPR simulation;

$$\delta_{dip}^{M.C.} = -\frac{\mu_0}{4\pi}\frac{g_e^2\mu_B^2 DG}{9(kT)^2} = -4.486\times10^{-3}\left(\frac{ppm}{cm^{-1}}\cdot cm^3\right)\times D\times G = -1.525\times10^{-4}\left(ppm\cdot cm^3\right)\times G$$

$$\delta_{dip}^{L.C.} = -\frac{g_e\beta D(2\Pi)}{9g_N\beta_N(kT)^2}\rho^{\pi} = -48.54\left(\frac{ppm}{cm^{-1}}\right)\times D\times\rho^{\pi} = -1.65(ppm)\times\rho^{\pi}$$

[b] Contact shifts was calculated by $\delta_{con} = \text{experimantal}\,(\delta_{iso}) - \text{calculated}\,(\delta_{dip}^{L.C.} + \delta_{dip}^{M.C.})$

[c] The unit for $\rho_{\alpha\beta}$ is au.

Table S9. Experimental isotropic shifts, estimated pseudocontact shifts and calculated Fermi contact spin densities with corresponding shifts for high-spin $Ni^{III}(OETPP^{\cdot})(Br)_2$ antiferromagnetically coupled with a_{2u} π cation radical. (chemical shift in ppm)

	δ_{iso}	δ_{dip}^{MC} [a]	δ_{dip}^{LC} [a]	ρ$^{\pi}$	G (cm^{-3})×10^{21}	δ_{con} [b]	$\rho_{\alpha\beta}$ [c]
			Ni(OETPP)Br$_2$, D = 0.034 cm^{-1}				
α-C	nd	0.0055	-0.0051	0.0031	-36.02	nd[j]	0.0018
β-C	342	0.0015	-0.0107	0.0065	-10.19	342	0.0032
meso-C	-416.1	0.0041	0.0289	-0.0175	-26.77	-416.1	-0.0036
q-C	206.2	0.0013	-	-	-8.76	206.2	0.0024
-C$\underline{H}_2$	47.8	0.0005	-	-	-3.43	47.8	-0.0002
-C$\underline{H}_3$	63.1	-0.0000	-	-	0.36	63.1	0.0007
o-C	-89.9	0.0008	-	-	-5.08	-89.9	-0.0027
m-C	4.8	0.0004	-	-	-2.73	4.8	-0.0001
p-C	-6.8	0.0003	-	-	-2.21	-6.8	-0.0003
-C$\underline{H}_2$	12.98	0.0005	-	-	-3.13	12.98	0.0004
-C$\underline{H}_3$	3.08	-0.0002	-	-	1.17	3.08	0.0000
o-H	3.47	0.0008	-	-	-4.92	3.47	0.0001
m-H	-1.58	0.0003	-	-	-1.89	-1.58	-0.0001
p-H	2.34	0.0002	-	-	-1.49	2.34	0.0001

[a] The calculated values of metal-centered and ligand-centered dipolar shifts were based on the zero-field splitting (D) which is mainly estimated from the datum of EPR simulation;

$$\delta_{dip}^{M.C.} = -\frac{\mu_0}{4\pi}\frac{g_e^2\mu_B^2 DG}{9(kT)^2} = -4.486\times10^{-3}\left(\frac{ppm}{cm^{-1}}\cdot cm^3\right)\times D\times G = -1.525\times10^{-4}(ppm\cdot cm^3)\times G$$

$$\delta_{dip}^{L.C.} = -\frac{g_e\beta D(2\Pi)}{9g_N\beta_N(kT)^2}\rho^{\pi} = -48.54\left(\frac{ppm}{cm^{-1}}\right)\times D\times\rho^{\pi} = -1.65(ppm)\times\rho^{\pi}$$

[b] Contact shifts was calculated by $\delta_{con} = \text{experimantal}\,(\delta_{iso}) - \text{calculated}\,(\delta_{dip}^{L.C.} + \delta_{dip}^{M.C.})$

[c] The unit for $\rho_{\alpha\beta}$ is au.

11. Diamagnetic NMR reference complex

Table S10. ^{1}H and ^{13}C NMR chemical shifts of the diamagnetic reference complex, $[Co(OETPP)(Im)_2](ClO_4)$,which is observed in $CDCl_3$ (in ppm).

S = 0	-C**H**$_2$-	-C**H**$_3$	*o*-H	*m*-H	*p*-H	*p*-CH_3
$[Co(OETPP)(Im)_2](ClO_4)$	2.07	-0.08	8.10	7.58	7.66	2.36[a]

	C_{meso}	C_α	C_β	*q-C*	*o*-C	*m*-C	*p*-C	-**C**H_2	-**C**H_3
	119.96	150.38	148.01	139.53	134.49	127.23	128.44	19.14	16.76

[a] observed from Zn(OETP(*p*-CH_3)P)

12. References

1. K. M. Barkigia, M. D. Berber, J. Fajer, C. J. Medforth, M. W. Renner and K. M. Smith, *J. Am. Chem. Soc.*, 1990, **112**, 8851.
2. B. Evans, K. M. Smith and J. H. Fuhrhop, *Tetrahedron Lett.*, 1977, **18**, 443.
3. J. S. Lindsey, I. C. Schreiman, H. C. Hsu, P. C. Kearney and A. M. Marguerettaz, *J. Org. Chem.*, 1987, **52**, 827.
4. M. W. Renner, K. M. Barkigia, D. Melamed, J.-P. Gisselbrecht, N. Y. Nelson, K. M. Smith and J. Fajer, *Res. Chem. Intermed.*, 2002, **28**, 741.
5. CrysAlisPro, *Version 1*, Agilent Technologies.
6. CrysAlisPro, *SCALE3 ABSPACK : A scaling algorithm for empirical absorption correction using spherical harmonics*, Oxford Diffraction, 2005.
7. G. M. Sheldrick, *SHELXL-97, NT Crystallographic System, release 6. 14; Bruker Analytical X-ray Systems: Madison, WI*, 2008.
8. S. Stoll and A. Schweiger, *J. Magn. Reson.*, 2006, **178**, 42.
9. R. J. Kurland and B. R. McGarvey, *J. Magn. Reson.*, 1970, **2**, 286.
10. J. Mispelter, M. Momenteau and J.-M. Lhoste, *J. Chem. Soc., Dalton Trans.*, 1981, 1729.
11. J. Mispelter, M. Momenteau and J.-M. Lhoste, in *Biological Magnetic Resonance*, eds. L. J. Berliner and J. Reuben, Plenum, New York, 1993, vol. 12.
12. I. Bertini, C. Luchinat and G. Parigi, *Solution NMR of Paramagnetic Molecules*, Elsevier, Amsterdam, 2001.
13. E. J. Baerends and P. Ros, *Int. J. Quantum Chem*, 1978, **14**, 169.
14. E. Van Lenthe and E. J. Baerends, *J. Comput. Chem.*, 2003, **24**, 1142.
15. W.-G. Han, T. Liu, T. Lovell and L. Noodleman, *J. Am. Chem. Soc.*, 2005, **127**, 15778.

16. R.-J. Cheng, P.-Y. Chen, T. Lovell, T. Liu, L. Noodleman and D. A. Case, *J. Am. Chem. Soc.*, 2003, **125**, 6774.